


## Special Issue Article

# An ultrahigh-throughput screening platform based on flow cytometric droplet sorting for mining novel enzymes from metagenomic libraries

Fuqiang Ma <sup>1\*</sup>, Tianjie Guo,<sup>1</sup> Yifan Zhang,<sup>1</sup>  
Xue Bai,<sup>2,3</sup> Changlong Li,<sup>1</sup> Zelin Lu,<sup>1</sup> Xi Deng,<sup>2</sup>  
Daixi Li,<sup>3</sup> Katsuo Kurabayashi<sup>4,5</sup> and Guang-yu Yang<sup>2\*\*</sup>

<sup>1</sup>CAS Key Lab of Bio-Medical Diagnostics, Suzhou Institute of Biomedical Engineering and Technology, Chinese Academy of Sciences, Suzhou, Jiangsu, 215163, China.

<sup>2</sup>State Key Laboratory of Microbial Metabolism, Joint International Research Laboratory of Metabolic and Developmental Sciences, School of Life Sciences and Biotechnology, Shanghai Jiao Tong University, Shanghai, 200240, China.

<sup>3</sup>Institute of Food Science and Engineering, University of Shanghai for Science and Technology, Shanghai, 200093, China.

<sup>4</sup>Department of Mechanical Engineering, University of Michigan, Ann Arbor, Michigan, 48109.

<sup>5</sup>Department of Electrical Engineering and Computer Science, University of Michigan, Ann Arbor, Michigan, 48109.

## Summary

**Uncultivable microbial communities provide enormous reservoirs of enzymes, but their experimental identification by functional metagenomics is challenging, mainly due to the difficulty of screening enormous metagenomic libraries. Here, we propose a reliable and convenient ultrahigh-throughput screening platform based on flow cytometric droplet sorting (FCDS). The FCDS platform employs water-in-oil-in-water double emulsion droplets serving as single-cell enzymatic micro-reactors and a commercially available flow cytometer, and it can efficiently isolate novel biocatalysts from metagenomic libraries by**

processing single cells as many as  $10^8$  per day. We demonstrated the power of this platform by screening a metagenomic library constructed from domestic running water samples. The FCDS assay screened 30 million micro-reactors in only 1 h, yielding a collection of esterase genes. Among these positive hits, Est WY was identified as a novel esterase with high catalytic efficiency and distinct evolutionary origin from other lipolytic enzymes. Our study manifests that the FCDS platform is a robust tool for functional metagenomics, with the potential to significantly improve the efficiency of exploring novel enzymes from nature.

## Introduction

Discovery of microbial enzymes with useful catalytic properties is of great importance for scientific, technological and biomedical applications. Laboratory microbial cultivation is a traditional method for microbial enzyme discovery. However, it recovers no more than 1% of the environmental microorganisms (Amann *et al.*, 1995), thus identifying a miniscule fraction of natural enzymes. In the past decade, metagenomics has emerged as a promising cultivation-independent approach for discovering candidate enzymes from microbial communities for various applications (Daniel, 2005; Lorenz and Eck, 2005; Simon and Daniel, 2011; Lee and Lee, 2013). Function-based metagenomic library screening is a powerful strategy in metagenomics to identify novel enzyme genes without relying on sequence homology. Its process involves heterologously expressing enzymes in a surrogate host and assaying enzyme activities with a screening substrate. This strategy is shown to enable the discovery of novel enzymes without precedent or enzymes catalysing unfamiliar reactions (Handelsman, 2004; Uchiyama and Miyazaki, 2009). In more recent years, Colin and coworkers have employed function-based metagenomics library screening to identify 42 new sulfate monoester and phosphotriester hydrolases representing three

Received 25 May, 2020; accepted 26 September, 2020. For correspondence. \*E-mail mafuqiang318@sibet.ac.cn; Tel. +86 512 69588303; Fax +86 512 69588303. \*\*E-mail yanggy@sjtu.edu.cn; Tel. +86 21 34207189; Fax +86 21 34207248.

protein superfamilies, most of which could not have been predicted by sequence-based analysis (Pierre *et al.*, 2015). Similarly, Liu *et al.* (2018) have identified 219 genes encoding carbohydrate-active enzymes (CAZymes) targeting cellulose, hemicellulose and pectin, which may provide novel biocatalysts for more efficient biomass utilization.

Despite its promise, function-based screening of metagenomic libraries still suffers from low efficiency, labor intensity and excessive time requirements. Specifically, the positive rates with metagenomic libraries are approximately one hit per 10 000–100 000 clones (Lorenz and Eck, 2005). This poses a challenge for identifying desired genes using conventional screening methods, such as agar plate assays and microtiter plate assays. Recently, the flow cytometric droplet sorting (FCDS) technique has been recognized as an efficient means for identify novel enzyme variants at the single-cell level (Chan *et al.*, 2017; Xu *et al.*, 2019). FCDS employs monodisperse pico-litre water-in-oil-in-water double emulsion droplets as single-cell micro-reactors, which encapsulate enzyme-expressing single cells, cell lysis agent and a fluorogenic substrate. Within the droplet micro-reactors, enzyme molecules are released to react with the fluorogenic substrate, producing fluorescent products. The fluorescence intensity of each droplet reflects the enzymatic activity in the droplet micro-reactor. Rapidly sorting the droplets based on their fluorescence signals with a commercial flow cytometer (several thousand events per second) allows for isolating enzyme genes with desired properties. Advanced modern flow cytometer instruments significantly bring promise to FCDS-based screening with their ultrahigh-throughput multi-parametric analysis capability, ease of use and wide availability (Lim and Abate, 2013; Zinchenko *et al.*, 2014; Larsen *et al.*, 2016; Chan *et al.*, 2017; Xu *et al.*, 2019). However, the bottleneck of FCDS exists against generating monodisperse water-in-oil-in-water double emulsion droplets that are compatible with flow cytometric analysis. These droplets are synthesized in a micro-channel on a microfluidic device. Ensuring effective wetting of the micro-channel walls with the continuous outer water phase is necessary for the secondary emulsification. However, modifying the hydrophilicity of the micro-channel surface is particularly challenging. Most current hydrophilic surface modification methods are complicated with multiple processing steps, thus limiting broad application of FCDS.

In this article, we developed a flexible and easy-to-operate two-step emulsification method to generate water-in-oil-in-water double emulsion droplets that were compatible with flow cytometric analysis. Our method employed a convenient and reliable hydrophilic modification approach to generate double emulsion droplets that use oxygen plasma treatment (Li *et al.*, 2016), which was

found to be remarkably effective in this study. Based on this method, we further built an FCDS system for function-based screening of metagenomic libraries and applied this screening platform to discover novel esterase genes from a metagenomic library constructed from running water samples. Our success in identifying a novel esterase from the domestic running water metagenome demonstrated the robustness of the FCDS platform as an efficient metagenomic library screening tool.

## Results

### *Two-step water-in-oil-in-water double emulsion droplet generation*

We used poly(dimethylsiloxane) (PDMS) microfluidic devices for droplet generation. Because native PDMS material is highly hydrophobic, its wettability needs to be turned hydrophilic for secondary emulsification. In this work, we employed an easy and reliable hydrophilic modification approach based on oxygen plasma treatment. To evaluate the effectiveness of this approach, we compared the wettability of PDMS material treated by different hydrophilic modification methods. As shown in Fig. S1, native PDMS is highly hydrophobic, with a contact angle of 105°. After oxygen plasma treatment, PDMS became highly hydrophilic, with a contact angle of only 19°. Its hydrophilicity was much higher than that of PDMS devices treated by sequential layer-by-layer deposition of polyelectrolytes (contact angle 63°), which has been considered one of the most convenient and efficient hydrophilic modification approaches (Bauer *et al.*, 2010; Zinchenko *et al.*, 2014). Glass material is natively hydrophilic and is an alternative for fabricating microfluidic devices, although with drawbacks such as a complicated and time-consuming fabrication process and high costs (Duffy *et al.*, 1998). Our results show that the hydrophilicity of plasma-treated PDMS was much higher than that of native glass (contact angle 57°). Better hydrophilicity should allow for more effective wetting of channel walls by the continuous outer water phase during secondary emulsification. Although the hydrophilicity of plasma-treated PDMS decreased over time during storage, its contact angle was still 60° (similar to native glass) even when exposed to air at room temperature for 4 h. Moreover, Li *et al.* (2016) reported that plasma-treated PDMS hydrophilicity could be stabilized by submersion in water, with a 33.9° contact angle after 72 h. Therefore, during double emulsion droplet generation, we expect the plasma-treated PDMS device to maintain high hydrophilicity for more than 4 h. Next, we bonded the plasma-treated PDMS slide with microfluidic channel features to a glass slide, obtaining a sealed hydrophilic microfluidic device. Employing this device, we observed continuous

and stable double emulsion droplet generation lasting for at least 10 h (data not shown). These results demonstrate that the plasma treatment approach could provide highly efficient hydrophilic modification and stable droplet generation for a long period.

Using the hydrophilic modification approach described above, we developed a reliable and convenient microfluidic two-step emulsification strategy, separating the first emulsification from the secondary emulsification, to generate water-in-oil-in-water double emulsion droplets. As illustrated in Fig. 1, first, water-in-oil single emulsion

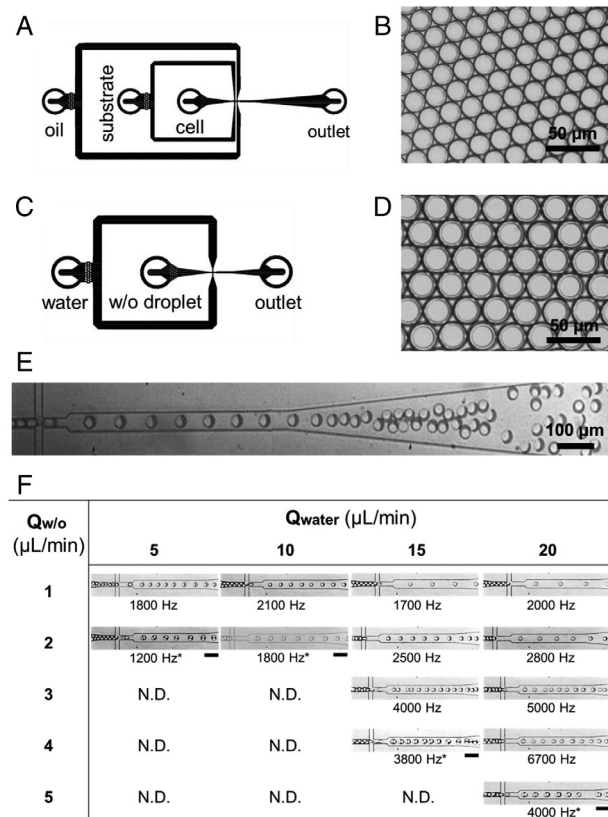


**Fig. 1.** Generation of water-in-oil-in-water double emulsion droplets using a two-step emulsification method. A. Design of the flow-focusing device with hydrophobic microchannels used for generating water-in-oil single emulsion droplets. This device contains two aqueous inlets that allow screening substrate and cell suspension to remain separated before droplet generation. B. Microscopic image of the water-in-oil single emulsion droplets formed in this procedure. C. Water-in-oil single emulsion droplets are re-injected into a second flow-focusing device with hydrophilic microchannels and dispersed into a continuous aqueous phase, forming water-in-oil-in-water double emulsion droplets. D. Microscopic image of the water-in-oil-in-water double emulsion droplets. E. Microscopic image taken by a high-speed camera showing the production of water-in-oil-in-water double emulsion droplets. F. The generation of water-in-oil-in-water double emulsion droplets under different flow rates for both outer water phase and water-in-oil single emulsion phase. Scale bars, 100 μm; N.D., water-in-oil-in-water double emulsion droplets were not stably generated; Asterisk indicates double-occupied water-in-oil-in-water double emulsion droplets were generated.

droplets were generated in a flow-focusing PDMS device treated by hydrophobic modification. This device has two aqueous phase inlets, allowing cell lysis reagent/substrate and cell suspension to be separated until droplet generation. We collected the single emulsion droplets into a 1-ml syringe and incubated them for cell lysis and enzymatic reaction. Subsequently, the syringe was vertically injected by a syringe pump and the water-in-oil emulsion in the top layer was re-injected into a second, hydrophilic chip, forming water-in-oil-in-water double emulsion droplets (Fig. 1C, Fig. S2).

Employing the two-step water-in-oil-in-water double emulsion droplet generation approach in this study, both droplet size and generation frequency can be flexibly controlled by varying the fluid flow rates. For water-in-oil single emulsion droplets generated with a 15-μm flow-focusing device, we adjusted the droplet diameter to vary from 17 to 33 μm, with a maximum generation frequency as high as 100 000 Hz (Fig. S3). For generating water-in-oil-in-water double emulsion droplets, as shown in Fig. 1F, the flow rates of the two fluids (continuous aqueous phase and single emulsion phase) affected the double emulsion droplet generation frequency as well as the thickness of the middle oil phase. As shown in Table S1, the thickness of the middle oil phase can be affected by the flow rates of both the aqueous phase and the water-in-oil phase. When the flow rates of the outer aqueous phase increase, the middle oil phase becomes thinner. While when the flow rates of the water-in-oil phase increase, the middle oil phase becomes slightly thicker. For flow cytometric analysis, double emulsion droplets with thinner middle oil phases were better suspended in the continuous aqueous phase, with lower sedimentation rates than droplets with a thicker middle oil phase (Arriaga *et al.*, 2015). Furthermore, controlling the middle oil phase thickness enabled generation of double emulsion droplets with a smaller diameter (similar to the diameter of the inner single emulsion droplet), which was beneficial for accommodating limits set by flow cytometer nozzle sizes (typically 70–100 μm, and the analyte particle diameter should be no more than one-third of the nozzle size). The generation frequency of double emulsion droplets ranged from 1700 to 6700 Hz, and higher single emulsion phase flow rates resulted in higher double emulsion droplet generation frequencies (Fig. 1F). However, further increases in single emulsion flow rates resulted in double-occupied double emulsion droplets.

#### Flow cytometric analysis of double emulsion droplets

For the analysis in a flow cytometer equipped with a 100-μm nozzle, we generated water-in-oil-in-water double emulsion droplets with a diameter of approximately 30 μm. The log dot-plot of forward scattering

(FSC) versus side scattering (SSC) of water-in-oil-in-water double emulsion droplets exhibits a distinct main population (red square in Fig. 2A), indicating that the double emulsion droplets were highly uniform. The high uniformity should be beneficial for precise discrimination of different enzymatic activities and accurate screening. To demonstrate this, we generated double emulsions with 0, 0.5, 1.0, 5.0, 20, 50 and 100  $\mu\text{M}$  of fluorescein. When analysed in the flow cytometer, we observed that the fluorescence intensity histograms of these emulsions could be clearly distinguished (Fig. 2B), suggesting that water-in-oil-in-water double emulsion droplets prepared by our two-step emulsification approach can be accurately discriminated on the basis of their fluorescence intensities, even when the difference between fluorescein concentrations are only twofold.

#### Enriching esterase genes from model libraries

To evaluate the capability of this ultrahigh-throughput screening platform to enrich for cells with esterase activity, we performed a model screening assay. First, we spiked cells expressing an *Archaeoglobus fulgidus* esterase (AFEST) into a large excess of cells expressing an inactive AFEST mutant (M4, a frame-shifted variant). The positive to negative ratios were set at 1:10, 1:100 and 1:1000. After droplet encapsulation and enzymatic reaction, populations producing high fluorescence signals were sorted by a flow cytometer (Fig. S4). The sorted cells were recovered and tested on LB agar plates containing 0.5% (vol./vol.) glyceryl tributyrate. Active wild-type AFEST colonies were distinguished from inactive M4 colonies by the transparent halos that formed around them (Fig. S4). The sorting enrichment factors were calculated by the change in WT to M4 ratio before and after

sorting. As shown in Table S2, positive cells with esterase activity were efficiently enriched, with an enrichment factor as high as 527-fold, even when the initial positive to negative ratio was as low as 1:1000. The model screening results indicated that our flow cytometric droplet screening system was able to successfully deliver positive genes.

#### Mining esterase genes from a running water metagenomic library

We next utilized the FCDS system to mine novel enzymes from metagenomic libraries. The workflow of this ultrahigh-throughput screening system (Fig. 3) involves extracting metagenomic DNA, digesting the DNA into fragments, cloning the DNA into expression vectors and transforming the DNA into a host strain to express proteins encoded by the inserts, which finally leads to creating a metagenomic library. Single cells from the library are encapsulated into double emulsion droplets, along with a fluorogenic substrate. After reaction, cells harbouring an esterase gene are sorted by flow cytometry and positive genes are verified by a secondary screening process.

We applied this FCDS system to mine novel esterases from a metagenomic library prepared from running water. Generally, one would expect domestic running water should not contain many microorganisms. However, this condition might change when the water pipeline becomes aged and corroded. Microorganisms would occupy the ecological niche especially at the junction of the water pipeline. These microorganism populations would be special because they are commonly resistant to bleaching agents (total chlorine at 0.05–4.0  $\text{mg L}^{-1}$  in China, National standard for tap water quality of the People's Republic of China) in running water. To this end, we would like to explore whether we can identify novel enzymes from the metagenomic library of running water using the FCDS system. This metagenomic library contained approximately 1 million clones, and the average size of the inserts was 2.5 kb. The entire metagenomic library contained 2500 Mbp of total sequence. Before cell encapsulation, we built a theoretical model based on the Poisson distribution. As shown in Table S3, it can be predicted that when the cell/droplet ratio is 1:10 (0.10), more than 90.5% droplets are empty and 9.5% droplets are cell-encapsulating droplets. The majority of these cell-encapsulating droplets are single-cell occupied (9.0% of total droplets and 94.7% of cell-encapsulating droplets). In addition, this percentage of single-cell-encapsulating droplets should be suitable for accurate and effective screening of enzyme libraries according to our previous work (Ma *et al.*, 2018). In this work, we encapsulated single cells from the library into water-in-oil-

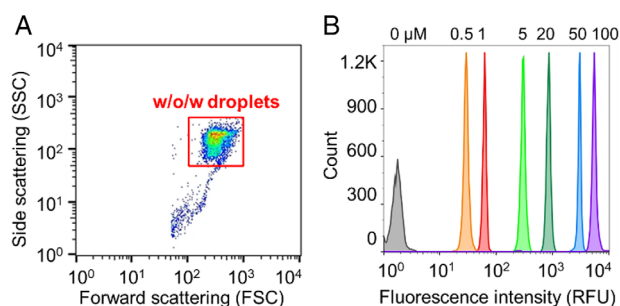


**Fig. 2.** Flow cytometric analysis of water-in-oil-in-water double emulsion droplets encapsulating various fluorescein concentrations. A. The log dot-plot of forward scattering (FSC) versus side scattering (SSC) of water-in-oil-in-water double emulsion droplets, indicating a distinct main population of monodisperse droplets. B. Overlay of fluorescence histograms of water-in-oil-in-water double emulsions containing different concentrations of fluorescein in their inner aqueous phase.

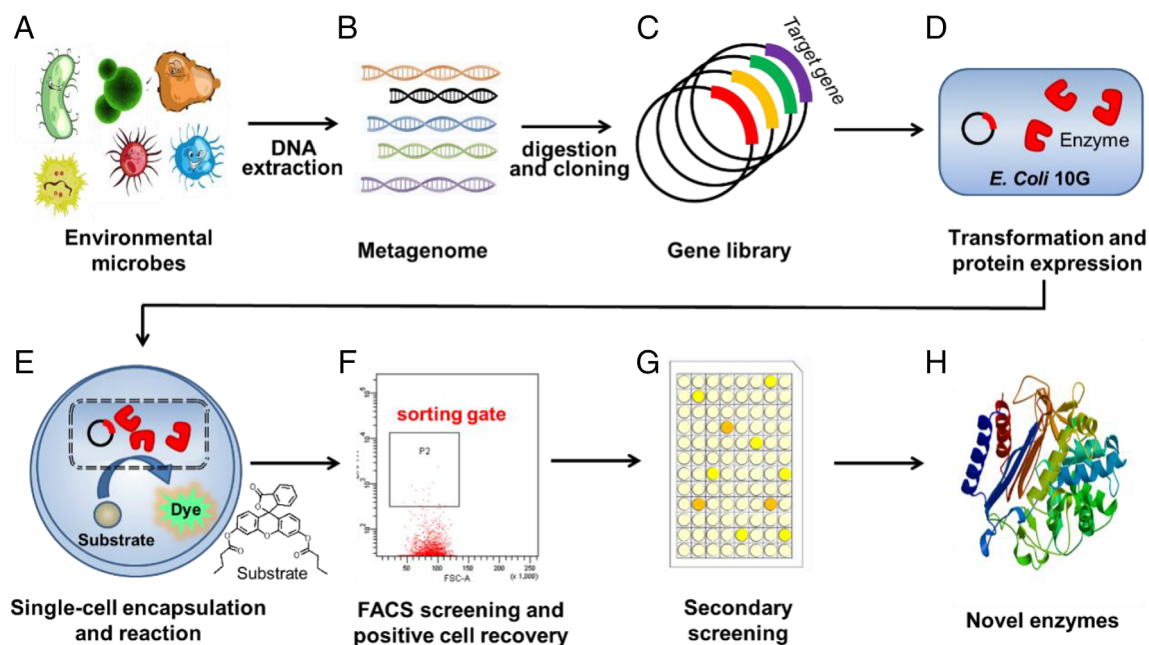


**Fig. 3.** Workflow of the ultrahigh-throughput screening platform based on flow cytometric droplet sorting to mine novel enzymes from metagenomic libraries. A. Collection of environmental microbes. B. Extraction of metagenomic DNA. C. Digestion and cloning of metagenomic DNA into an expression vector. D. Transformation of recombinant plasmids into a host strain for encoded protein expression. E. Encapsulation of single cells into water-in-oil-in-water double emulsion droplets, along with the screening substrate. F. Flow cytometric analysis and sorting of positive droplets. G. Secondary screening based on 96-well plate assays. H. Identification of novel enzymes.

in-water double emulsion droplets at a cell to droplet ratio of 1:10 to ensure that 95% of the cell-containing droplets were single-cell occupied. We observed that the experimental encapsulating effect fits well with the theoretical model, the majority cell-encapsulating droplets were single cell (Fig. S5) with a single-cell occupation of approximately 96.2% in cell-encapsulating droplets and 6.6% of total droplets (2000 droplets sampled in total). Employing the FCDS ultrahigh-throughput screening system, we screened 30 million droplets in a total of only 1 h to cover approximately 95% of the metagenomic library diversity. Subsequently, 180 sorted clones were tested by secondary screening based on a 96-well plate assay, yielding 21 positive clones that exhibited esterase activities. Sequences of the metagenomic inserts of these positive clones revealed that each clone contained a putative open reading frame. Through sequence analysis, we found that there were only four total gene types and most of them were repeatedly identified, indicating that the metagenomic library had been exhausted through our ultrahigh-throughput screening approach. We noticed that the positive rate in our case was relatively low (four out of one million colonies). This was probably due to the high sorting threshold we used during screening, which might have neglected esterases with lower activity. The four positive genes were named Est A, Est B, Est C

and Est WY (Table S4). Protein sequences for these esterases are shown in Table S5.

As shown in Table S4, Est A, Est B and Est C are identical to existing protein sequences in the NCBI database. Est A is identical to a *pimeloyl-ACP methyl ester esterase BioH* from *Shigella flexneri* (accession number WP\_001060072.1). Est B is identical to an esterase from *Escherichia coli* (accession number PSY02120.1). Est C is identical to an esterase from an uncultured bacterium (accession number AHK13303.1). For Est WY, in contrast, there were no identical proteins in the NCBI database. The closest proteins to Est WY were a serine hydrolase from *Variovorax* sp. *JS1663* (accession number WP\_086925844.1, sequence identity 84.21%), a serine hydrolase from *Mitsuaria chitosanitabida* (accession number WP\_148661411.1, sequence identity 72.82%) and a serine hydrolase from *Ramlibacter rhizophilus* (accession number WP\_135283256.1, sequence identity 63.31%). Est WY should belong to the same family as these serine hydrolases. However, the enzymatic properties of all of these enzymes have not been characterized. We cloned *est wy* gene into pET28a vector, transformed the recombinant plasmid into *E. coli* BL21 (DE3), and expressed this enzyme in LB medium. We further purified Est WY protein (Fig. S6) and characterized its basic enzymatic properties, including substrate specificity, optimal temperature, thermostability and optimal pH (Fig. 4).

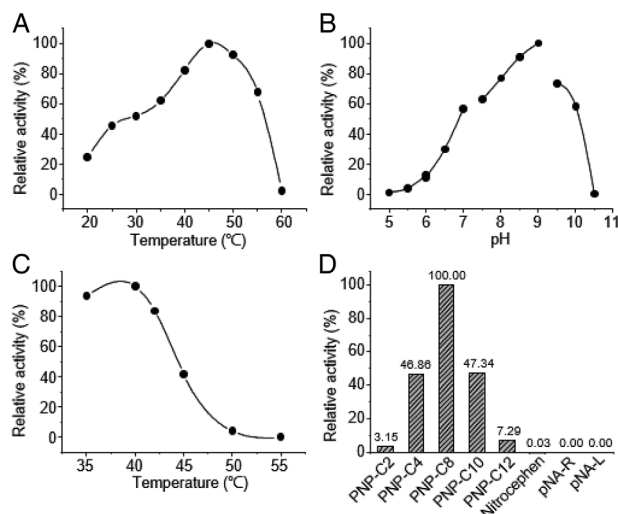


**Fig. 4.** Enzymatic properties of Est WY. A. The optimal temperature of Est WY. The measurement was performed using p-nitrophenol butyrate as the substrate at pH 9.0. The relative activity of Est WY at different temperatures was normalized to its specific activity at 45°C. B. The optimal pH of Est WY. The measurement was performed using p-nitrophenol butyrate as the substrate at 37°C. The relative activity at different pH values was normalized to the specific activity at pH 9.0. C. The residue activity of Est WY after incubated at different temperatures for 15 min. The relative activity after incubation at different temperatures was normalized to the specific activity incubated at 40°C for 15 min. D. Substrate specificity of Est WY. The specificity activity toward different substrates was normalized to that toward p-nitrophenol octanoate.

We found that Est WY was an efficient esterase, with a specific activity as high as 20 U mg<sup>-1</sup> at 37°C toward p-nitrophenol octanoate (pH 9.0). Furthermore, Est WY was a mesophilic enzyme with an optimal temperature of 45°C and optimal pH value of 9.0 (Fig. 4A and B). The  $T^{15}_{1/2}$  of Est WY was estimated at approximately 45°C (Fig. 4C). The optimal substrate of Est WY was p-nitrophenol octanoate (Fig. 4D). We also found that Est WY exhibited relatively weak  $\beta$ -lactamase activity, and its specific activity toward nitrocephen was 0.05 U mg<sup>-1</sup>. However, Est WY was inactive with amidase and peptidase substrates, such as L-Arginine p-nitroanilid and L-Leucine p-nitroanilide.

We further measured the kinetic parameters of Est WY toward four ester substrates (pNP esters) and a beta-lactamase substrate (nitrocephen). As shown in Table 1, Est WY has much higher catalytic activity toward ester substrates than that toward beta-lactamase substrate. The catalytic efficiency ( $k_{cat}/K_M$ ) toward nitrocephen is 3430-folds lower than that toward pNP-C8. Therefore, Est WY should be an esterase with promiscuous lactamase activity.

To study the taxonomic location of Est WY in the lipolytic enzyme superfamily, we analysed the phylogenetic relationship based on esterase/lipase classification, including

**Table 1.** Kinetic parameters of Est WY toward both ester substrates (pNP-C2 ~ pNP-C10) and beta-lactamase substrate (nitrocephen).

Substrate	$k_{cat}$ (s <sup>-1</sup> )	$K_M$ (mM)	$k_{cat}/K_M$ (mM <sup>-1</sup> s <sup>-1</sup> )
pNP-C2	28.85	0.52	55.48
pNP-C4	199.98	0.28	714.21
pNP-C8	121.83	0.053	2298.68
pNP-C10	199.92	0.21	952.0
Nitrocephen	0.58	0.86	0.67

Note: pNP, p-nitrophenol; pNP-C2, p-nitrophenol acetate; pNP-C4, p-nitrophenol butyrate; pNP-C8, p-nitrophenol octanoate; pNP-C10, p-nitrophenol decanoate. The kinetic parameters were measured at 37°C.

the previously reported families (Arpigny and Jaeger, 1999). As shown in Fig. 5, Est WY, along with its homologues, WP\_148661411.1 and WP\_135283256.1 (two of the closest sequences in NCBI, with sequence identities of 84.21% and 63.31% respectively, as described above), were divided into a separate branch. All sequence identities between Est WY and members of known lipolytic families were less than 35%. These results indicated that Est WY was a novel esterase with a distinct evolutionary origin from other lipolytic enzymes.

We further investigated the three-dimensional characteristics of Est WY. Structural models of Est WY were constructed employing the SWISS-MODEL engine (<https://swissmodel.expasy.org/>) (Waterhouse *et al.*, 2018). Searching for templates from the SWISS-MODEL crystal structure library, we chose two templates with the highest sequence identities with Est WY for modelling. These two templates were Est U1 from an uncultured bacterium (SMTL ID: 4ivk.1, sequence identity 33%) and Est-Y29 from a metagenome (SMTL ID: 5zvw.1, sequence identity 35%). The quality of the two Est WY models constructed with these two templates was estimated by their GMQE scores (ranging from 0 to 1, higher scores indicating better quality) (Waterhouse *et al.*, 2018). The GMQE scores of both models were 0.7, suggesting that both models were reliable. Although the sequence identity between these two templates was merely 29%, we found that the models based on them were highly similar in structural organization, with an RMSD of 1.513 Å when performing superposition of equivalent C $\alpha$  atoms (Fig. 6A). The Est WY models contained a seven-stranded antiparallel  $\beta$ -sheet with several  $\alpha$ -helices on one face, and the catalytic serine residue was located at the beginning of an  $\alpha$ -helix adjacent to the central sheet (Fig. 6B). These features reveal that the Est WY models include the  $\beta$ -lactamase fold, which is distinct from the fold of most lipolytic enzymes. Furthermore, we predicted Est WY catalytic residues by comparing the Est WY models with their relative templates (Fig. S7). Est WY contains a Ser-Lys-Tyr (Ser62, Lys65 and Tyr178,

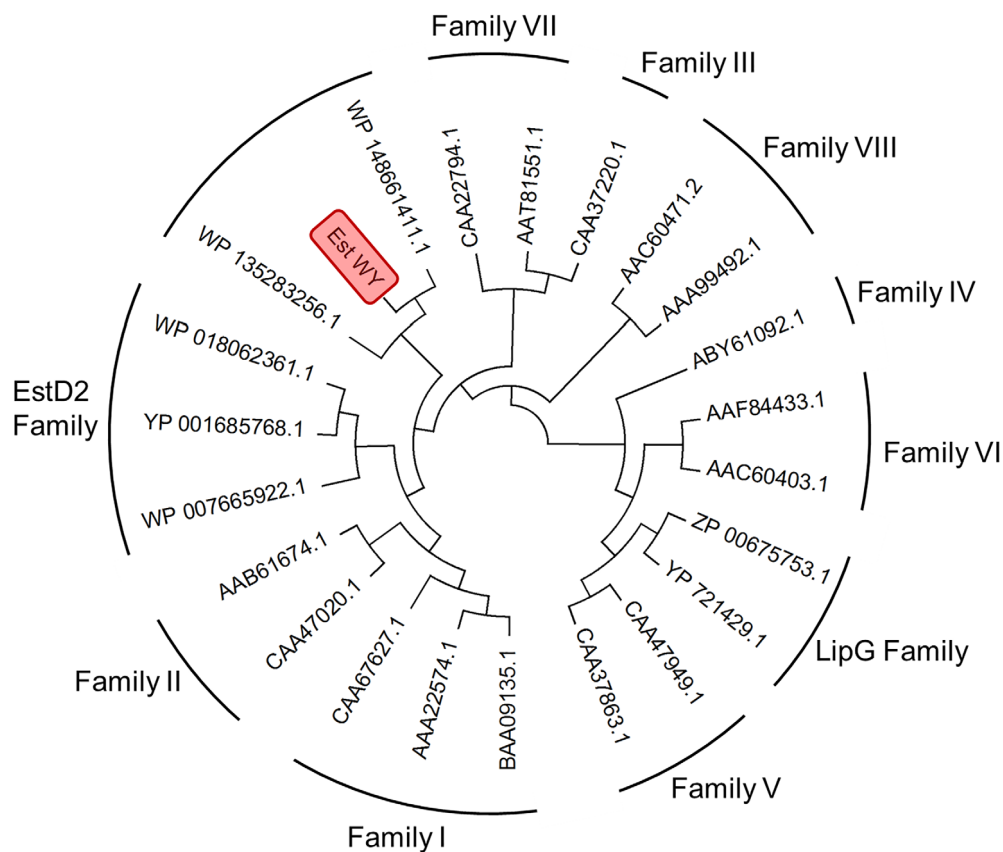


**Fig. 5.** Phylogenetic analysis of Est WY and typical lipolytic enzymes. The tree was constructed in MEGA7 by using the Maximum Likelihood method based on the JTT matrix-based model. Est WY was grouped with two of the closest proteins in NCBI, WP\_148661411.1 and WP\_135283256.1.

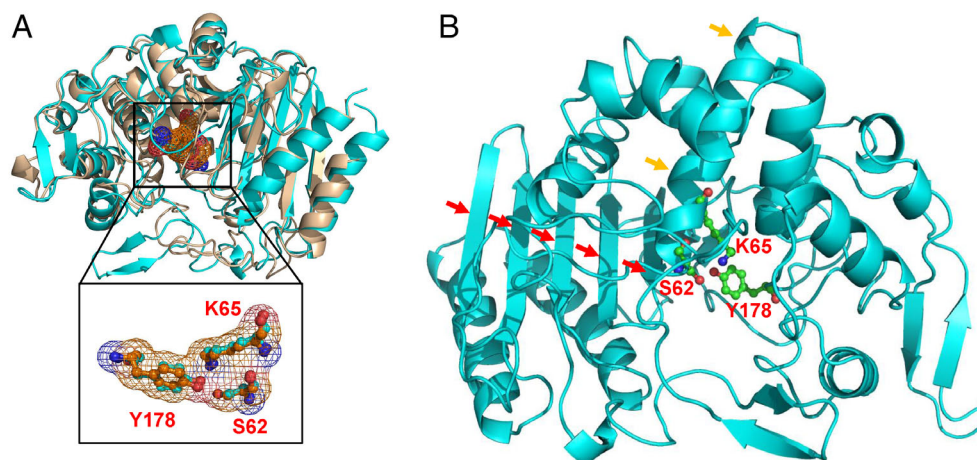


**Fig. 6.** Modelling the structure of Est WY. A. Superposition of two Est WY models constructed from two different templates (Est U1 and Est-Y29), with an RMSD value of 1.513 Å. The Est WY model constructed from Est U1 is shown in cyan and the EstWY model constructed from Est-Y29 is shown in light orange. The overall structures of both models are shown in cartoon format. Residues in the black square identify the Ser-Lys-Tyr catalytic triad, and the catalytic triads of the two models are highly similar in spatial arrangement (RMSD 0.228 Å). B. Folding and catalytic triad of Est WY model constructed with Est U1. The Ser-Lys-Tyr catalytic triad is shown in stick-and-ball format in green. The model contains a seven-stranded antiparallel  $\beta$ -sheet (indicated by red arrows) with several  $\alpha$ -helices on one face. The catalytic serine residue is located at the beginning of an  $\alpha$ -helix (indicated by orange arrows) adjacent to the central sheet.

Fig. 6) catalytic triad instead of the Ser-Asp-His triad that is commonly shared in other lipolytic enzymes, except Family VIII (Cha *et al.*, 2013; Renko *et al.*, 2014). Moreover, the Ser-Lys-Tyr catalytic triad is conserved in Est WY and its homologues on the same phylogenetic branch (Fig. S8). All these features reveal that Est WY is a novel lipolytic enzyme; however, whether it belongs to an existing family or represents a new family will require further study and should be carefully determined.

## Discussion

Due to remarkable advantages, such as ultrahigh-throughput, wide availability, user-friendliness and multi-parametric analysis capability, the FCDS technique has drawn broad attention as a promising means for screening various biological and physiological targets at a single-cell level. Several exciting applications have been demonstrated using the FCDS technique. For example, Larsen *et al.* (2016) developed an FCDS-based optical polymerase sorting technique as a general strategy for expanding polymerase function. Zhu and coworkers extended the scope of FCDS applications to detect metabolites and employed this system to screen high lactic acid-producing *Bacillus coagulans* mutant strains (Xu *et al.*, 2019). The advantages of recently developed FCDS systems as well as their potential applications are summarized in Table 2.

However, the lack of easy and reliable methods for generating water-in-oil-in-water double emulsion droplets has severely limited wide-scale applications of FCDS. The key component of double emulsion droplet generation is hydrophilic modification of microfluidic devices for the secondary emulsification. Scientists have developed several strategies for obtaining hydrophilic microfluidic devices (Table 2). The most straightforward approach is fabricating devices with materials that are natively hydrophilic, such as glass and silicon (Jing *et al.*, 2013; Lim and Abate, 2013; Zinchenko *et al.*, 2014; Larsen *et al.*, 2016; Chan *et al.*, 2017; Xu *et al.*, 2019). However, the fabrication of glass or silicon microfluidic chips is complicated, time-consuming and expensive (Duffy *et al.*, 1998), making those materials less desirable. By contrast, microfluidic device fabrication using PDMS is widely adopted owing to its rapid manufacturability, high flexibility and low cost (Duffy *et al.*, 1998; McDonald and Whitesides, 2002). These advantages have driven the development of a wide range of hydrophilic modification approaches for PDMS devices. These approaches include UV/ozone treatment (Efimenko *et al.*, 2002; Chen and Lahann, 2005), chemical vapour deposition (Lahann *et al.*, 2003; Chen *et al.*, 2008), sol-gel methods

(Abate and Weitz, 2009), chemical grafting by plasma polymerization (Barbier *et al.*, 2006; Dhananjay and Chantal, 2006) and layer-by-layer deposition (Wang *et al.*, 2006). Unfortunately, all these methods are still complicated and involve multiple processing steps, rendering hydrophilic modification of PDMS devices time-consuming, unreliable and difficult to implement, especially when surface modification is partially patterned.

In this work, we developed a convenient and reliable hydrophilic modification approach using oxygen plasma treatment. To achieve hydrophilic modification of PDMS devices, we sealed microfluidic channels in a PDMS layer with a glass slide after oxygen plasma treatment under optimized conditions. We observed that the fabricated PDMS device was highly hydrophilic and could be used immediately for secondary emulsification without any further modification. It is reported that the hydrophilicity of PDMS devices obtained through plasma treatment is temporary (Trantidou *et al.*, 2017). However, our research has affirmed that the hydrophilicity lifetime is sufficient to allow for the whole secondary emulsification process, enabling at least 10 h of stable water-in-oil-in-water double emulsion droplet generation. To the best of our knowledge, the plasma treatment approach is one of the most convenient and efficient hydrophilic modification methods for PDMS devices. With the easy, reliable and convenient operation, the double emulsion droplet generation method employing plasma treatment could be easily adopted by most laboratories, which would significantly promote expanded applications of FCDS.

On the basis of our results, we next applied the FCDS platform for functional screening of metagenomic libraries constructed from domestic running water (Table 1). After screening 30 million clones at a speed of 10 000 events per second, we identified four esterase genes. Further phylogenetic and 3D structural modelling revealed that one of these esterases, Est WY, was a novel esterase with high catalytic efficiency and distinct evolutionary origin from other lipolytic enzymes. Our successful identification of novel esterase genes manifests that FCDS is a robust platform for functional screening of metagenomic libraries.

## Experimental procedures

### Chemicals and materials

The materials used were purchased from Sigma-Aldrich unless otherwise noted. Fluorinated oil containing surfactant for water-in-oil single emulsion droplet generation was purchased from Bio-Rad. Sylgard 184 PDMS kit for microfluidic device fabrication was purchased from Dow Corning.



**Table 2.** Recent development of FCSM techniques and their applications.

Entry	W/o/w droplet generation strategy	Hydrophilic modification method	Flow cytometric sorting rate (kHz)	Application	References
1	One-step emulsification with a flow-focusing PDMS device	Layer-by-layer deposition of a polyelectrolyte multilayer (partially patterned)	No sorting performed	Analysing droplets with varying fluorophore concentrations	Jing <i>et al.</i> (2013)
2	Two-step emulsification with PDMS devices with non-planar geometry	Hydrophobic devices without modification (special device geometry)	10	Enrichment of droplets with different fluorophores	Lim and Abate (2013)
3	Two-step emulsification using two flow-focusing PDMS devices	Coated with poly-electrolytes (whole device)	10–15	Enrichment of active arylsulfatase clones from low-activity variants	Zinchenko <i>et al.</i> (2014)
4	Two-step emulsification using two quartz glass devices	Hydrophilic devices without modification	5–8	Evolving a manganese-independent TNA polymerase	Larsen <i>et al.</i> (2016)
5	One-step emulsification with a flow-focusing PDMS device	Two-step sol-gel coating (partially patterned)	Not mentioned	Enrichment of functionally correct GFP genes from <i>E. coli</i> strain	Chan <i>et al.</i> (2017)
6	One-step W/O/W microdroplets generator	Coating with PEG-200 (partially patterned)	0.1–0.5	Screening high lactic acid-producing <i>Bacillus coagulans</i> mutant strains	Xu <i>et al.</i> (2019)
7	Two-step emulsification with two flow-focusing PDMS devices	Oxygen plasma treatment (whole device)	10	Functional screening of metagenomic library	This work

### Equipment

The fluids were driven by Harvard Phd Ultra syringe pumps (Harvard Apparatus, USA) for droplet generation. A Nikon Ti inverted microscope (Nikon, Japan) equipped with a Phantom M110 high-speed camera (Vision Research, USA) was used to detect the formation of droplets. Flow cytometry analysis and sorting of water-in-oil-in-water double emulsion droplets were performed on a BD FACSAriaII (Becton-Dickinson, USA) flow cytometer which was operated by a BD FACSDiva software (Becton-Dickinson).

### Characterization of the wettability of different materials

To evaluate the effect of hydrophilic modification on PDMS, we compared the wettability of native PDMS, native glass, PDMS modified by sequential layer-by-layer deposition of polyelectrolytes (Bauer *et al.*, 2010; Zinchenko *et al.*, 2014), PDMS treated with oxygen plasma and plasma-treated PDMS exposed to air at room temperature for different period of time. We took images of a 2- $\mu$ l droplet of distilled water on the surface of different materials using a stereomicroscope. And the value of contact angles was measured with ImageJ (Fiji).

### Microfluidic device design and fabrication

Microfluidic devices for droplet generation were designed according to Prof. Florian Hoffelder and his coworkers' design (<http://www2.bio.cam.ac.uk/~fhlab/dropbase/dropgen.php>) (Zinchenko *et al.*, 2014). The devices were fabricated in PDMS using soft lithography techniques (Xia and Whitesides, 1998). The device master was fabricated by coating a layer of SU-2025 (20  $\mu$ m) on a silicon wafer using photolithography. The master was attached to the bottom of a plastic Petri dish and covered with a mixture of PDMS and curing agent at the ratio of 9:1 (wt./wt.). After degassing and curing at 70°C for 6 h the PDMS device was peeled off from the master, the device was cut into single units and holes for tubing (0.75-mm outer diameter) connections were created using a 0.75-mm punch. The single unit for droplet generation with micro-channel features was then sealed with a glass slide after treating with oxygen plasma (COVANCE-1MP, Femto Science) for 60 s at a plasma generation power of 50 W.

For generating water-in-oil single emulsion droplets, the channel walls of microfluidic chips were made hydrophobic by coated with a hydrophobic surface agent trichloro (1H,1H,2H,2H-perfluorooctyl) silane (Sigma-Aldrich) in fluorinated oil HFE-7500 (2%, vol./vol.; 3M). To produce hydrophilic chips for generating water-in-oil-in-water double emulsion droplets, PDMS devices were treated with oxygen plasma treatment, namely, the

chips were used immediately after sealing with a glass slide.

#### *Metagenomic gene library creation and single-cell encapsulation*

The microbes in 5 L domestic running water were collected using a 2- $\mu\text{m}$  filter paper, and the total genomic DNA was extracted as described previously (Gabor *et al.*, 2003). Briefly, the collected cells were re-suspended in 1 ml lysis buffer, which contained lysozyme (50 mg ml<sup>-1</sup>) and proteinase K (10 mg ml<sup>-1</sup>). The mixture was incubated at 37°C for 30 min. The lysis was terminated by adding 0.1 ml of 20% SDS and then incubated for 2 h at 65°C. Chloroform extraction and isopropanol precipitation were performed to extract genomic DNA. The DNA precipitate was harvested and dissolved in 100  $\mu\text{l}$  TE buffer. The genomic DNA was subsequently digested with the restriction enzyme *Bsp*143I. DNA fragments with sizes of 1–3 kb were isolated by gel electrophoresis and cloned into the *Bam*HI site of pUC18. The recombinant plasmid library was then transformed into *E. coli* 10G strain. For protein expression, the bacteria pool was inoculated into LB medium and incubated at 37°C, 220 rpm. To express the proteins encoded by the metagenomic library, isopropyl  $\beta$ -D-thiogalactoside (IPTG) was added to a final concentration of 0.5 mM when the OD<sub>600nm</sub> of cell culture reached 0.6–0.8. The bacteria were cultured at 25°C for 16 h.

Before single-cell encapsulation, cell suspension was prepared as described previously (Ma *et al.*, 2014). Briefly, 1 ml cell culture was collected, washed with 10 mM Tris–HCl (pH 8.0) twice and then re-suspended in 1 ml of Tris–HCl. Cell density was adjusted by dilution to obtain the required cell/droplet ratio after encapsulation according to Poisson distribution (Köster *et al.*, 2008). A two-aqueous-phase flow-focusing PDMS device with hydrophobic modification was employed for single-cell encapsulation. Fluorescein dibutyrate (Sigma-Aldrich) employed as a fluorogenic esterase substrate was co-encapsulated with cell suspension to a final concentration of 1.0 mM. To achieve the cell/droplet ratio of 1:10 in our experiment, we adjusted the cell concentration based on the assumption that 1 ml of *E. coli* suspension at OD<sub>600 nm</sub> = 1 would contain  $5 \times 10^8$  cells (Agresti *et al.*, 2010). For water-in-oil single emulsion droplet generation, the cell concentration was adjusted to OD<sub>600 nm</sub> = 0.1, and the flow rates of the cell suspension, the screening substrate solution and the oil phase were 2, 2 and 5  $\mu\text{l min}^{-1}$  respectively. We evaluated the cell-encapsulation efficiency under a 40 $\times$  objective of a microscope. The generated single emulsion droplets were collected and incubated on a thermo-shaker at 37°C for a period of

time. After incubation, the reaction was stopped on ice and re-injected to a flow-focusing PDMS device with hydrophilic modification, forming water-in-oil-in-water double emulsion droplets, which were further subjected to FACS assays.

#### *Droplet generation*

For water-in-oil single emulsion droplet generation, cell suspension and screening substrate solution for esterase were used as aqueous phases, which were mixed with a ratio of 1:1 before the flow-focusing junction and subsequently dispersed into the droplet generation oil (Bio-Rad, QX200 DG Oil for EvaGreen, 1864005) at the flow-focusing junction. During droplet generation, both the flow rates of cell suspension and screening substrate solution were 2  $\mu\text{l min}^{-1}$ , and the flow rate of oil phase was 5  $\mu\text{l min}^{-1}$ . For generating water-in-oil-in-water double emulsion droplets, 10 mM Tris–HCl (pH 8.0) containing 1% (wt./vol.) Tween 80 was used as the continuous aqueous phase for dispersing water-in-oil single emulsion droplets. To optimize the generation of double emulsion droplets, the flow rate of single emulsion phase was adjusted between 1 and 5  $\mu\text{l min}^{-1}$ , and the continuous aqueous phase adjusted between 5 and 20  $\mu\text{l min}^{-1}$ . Before injected into PDMS devices, all the fluids except the water-in-oil single emulsion were filtered by a 2- $\mu\text{m}$  syringe filter.

#### *Flow cytometric analysis and sorting of double emulsion droplets*

For flow cytometric analysis and sorting, the water-in-oil-in-water double emulsion droplets were diluted into 10 mM Tris–HCl (pH 8.0) containing 0.1% (wt./vol.) Tween 80 and loaded into flow cytometry equipped with a 100- $\mu\text{m}$  nozzle using PBS as sheath fluid. The fluorescence of the enzymatic product, fluorescein, was excited with a 488-nm laser and the emission was detected employing a  $530 \pm 30$  nm band-pass filter. The analysing and sorting rate was set at  $\sim 10\,000$  events per second. The double emulsion population was gated on logFSC/logSSC in the sample and the sorter was triggered on product fluorescence (FITC channel) (Fig. S4). The sorted sample was collected into a 2-ml Eppendorf tube containing 1 ml LB medium (without antibiotic). To recover positive cells, the sorted double emulsion droplets were incubated at 37°C for 1 h, and subsequently cultured on agar plates containing ampicillin. The esterase activity of each colony was detected in 96-well plates using 4-nitrophenyl butyrate as the substrate.

### Model screening

The *E. coli* 10G cells expressing an esterase AFEST (Manco *et al.*, 2000) in cytoplasm were mixed with *E. coli* 10G cells harbouring empty pUC18 plasmid at ratios of 1:10, 1:100 and 1:1000 respectively. The cell mixtures were encapsulated into water-in-oil-in-water double emulsions with fluorescein dibutyrate. After incubation at 37 °C for 30 min, the samples were analysed in a flow cytometer and the population with the highest fluorescence intensity was sorted and collected into 2-ml Eppendorf tubes containing 1 ml LB medium (without antibiotic). The collected sample was incubated at 37 °C for 1 h for recovery. Subsequently, the sample was cultured on agar plates containing 1 mM triglyceride butyrate, which was dispersed by phacoemulsification. After growing overnight, negative and positive colonies can be distinguished according to the transparent haloes formed by the hydrolysis of AFEST. The enrichment factors were calculated according to the positive/negative cell ratios before and after sorting.

### Clone, over-expression and purification of Est WY

We re-cloned *est wy* gene into pET28a vector (Novagen, Madison, WI, USA), transformed the recombinant plasmid into *E. coli* BL21 (DE3). For protein expression, the transformed cells were grown in LB medium containing kanamycin (0.05 mg m<sup>-1</sup>) at 37 °C until OD<sub>600nm</sub> of the medium reached 0.8. Then the protein expression was induced by adding IPTG at a final concentration of 1.0 mM and then the medium was cultured at 25 °C, 220 rpm for 18 h. The cells were harvested by centrifugation and Est WY protein was purified using Ni-column affinity chromatography as described previously (Ishmukhametov *et al.*, 2005).

### Characterization of the enzymatic properties of Est WY

The specific activity of Est WY toward 4-nitrophenyl acetate (pNP-C2), 4-nitrophenyl butyrate (pNP-C4), 4-nitrophenyl octanoate (pNP-C8), 4-nitrophenyl laurate (pNP-C12) and 4-nitrophenyl palmitate (pNP-C16) was measured by monitoring the increasing absorbance of the reaction mixture at OD<sub>405nm</sub>, using a UV2600 spectrophotometer (Shimadzu). The specific activity of Est WY toward L-Leucine p-nitroanilide and L-Arginine p-nitroanilide was measured at OD<sub>380nm</sub>. The specific activity of Est WY toward nitrocephen was measured at OD<sub>500nm</sub>. All the final substrate concentrations were 1 mM. One unit was defined as the enzyme quantity that produced 1 μmol of product per minute under the above reaction conditions.

The optimal temperature of Est WY was measured by incubating the reaction mixture at different temperatures, ranging from 20 °C to 60 °C. To study the thermostability (T<sup>15</sup><sub>1/2</sub>) of Est WY, Est WY protein (1 mg ml<sup>-1</sup>) was incubated at different temperatures (ranging from 30 °C to 60 °C) for 15 min and then transferred on ice immediately. The residue activity was determined at 37 °C employing 4-nitrophenyl butyrate as the substrate (final concentration 1 mM). T<sup>15</sup><sub>1/2</sub> was estimated according to the inactivation curve.

The optimal pH of Est WY was measured in different buffers with a series of pH values from 5.0 to 11.0, including sodium acetate buffer (pH 5.0, 5.5, and 6.0), sodium phosphate buffer (pH 6.0, 6.5 and 7.0), Tris-HCl buffer (pH 7.5, 8.0, 8.5 and 9.0) and CAPS buffer (pH 9.5, 10.0, 10.5 and 11.0). The measurement was performed at 37 °C and 4-nitrophenyl butyrate was employed as the test substrate (final concentration 1 mM).

### Acknowledgements

This work was supported by the National Natural Science Foundation of China (Grant Nos. 31900911 and 21627812), Jiangsu Basic Research Plan of Natural Science (Grant No. SBK2019041665) and China Postdoctoral Science Foundation (Grant No. 2019 M660129).

### Data Availability Statement

The DNA sequence of the novel esterase identified in this work, Est WY, has been submitted to GenBank and the accession number is MN722427.

### References

- Abate, A., and Weitz, D. (2009) High-order multiple emulsions formed in poly(dimethylsiloxane) microfluidics. *Small* **5**: 2030–2032.
- Agresti, J., Antipov, E., Abate, A., Ahn, K., Rowat, A., Baret, J., *et al.* (2010) Ultrahigh-throughput screening in drop-based microfluidics for directed evolution. *Proc Natl Acad Sci U S A* **107**: 4004–4009.
- Amann, R., Ludwig, W., and Schleifer, K. (1995) Phylogenetic identification and in situ detection of individual microbial cells without cultivation. *Microbiol Rev* **59**: 143–169.
- Arpigny, J., and Jaeger, K. (1999) Bacterial lipolytic enzymes: classification and properties. *Biochem J* **343**: 177–183.
- Arriaga, L., Amstad, E., and Weitz, D. (2015) Scalable single-step microfluidic production of single-core double emulsions with ultra-thin shells. *Lab Chip* **15**: 3335–3340.
- Barbier, V., Tatoulian, M., Li, H., Arefi-Khonsari, F., Ajdari, A., and Tabeling, P. (2006) Stable modification of PDMS surface properties by plasma polymerization: application to the formation of double emulsions in microfluidic systems. *Langmuir* **22**: 5230–5232.

- Bauer, W., Fischlechner, M., Abell, C., and Huck, W. (2010) Hydrophilic PDMS microchannels for high-throughput formation of oil-in-water microdroplets and water-in-oil-in-water double emulsions. *Lab Chip* **10**: 1814–1819.
- Cha, S., An, Y., Jeong, C., Kim, M., Jeon, J.H., Lee, C., *et al.* (2013) Structural basis for the  $\beta$ -lactamase activity of EstU1, a family VIII carboxylesterase. *Proteins* **81**: 2045–2051.
- Chan, H., Ma, S., Tian, J., and Leong, K. (2017) High-throughput screening of microchip-synthesized genes in programmable double-emulsion droplets. *Nanoscale* **9**: 3485–3495.
- Chen, H., and Lahann, J. (2005) Fabrication of discontinuous surface patterns within microfluidic channels using photodefinable vapor-based polymer coatings. *Anal Chem* **77**: 6909–6914.
- Chen, H., McClelland, A., Chen, Z., and Lahann, J. (2008) Solventless adhesive bonding using reactive polymer coatings. *Anal Chem* **80**: 4119–4124.
- Daniel, R. (2005) The metagenomics of soil. *Nat Rev Microbiol* **3**: 470–478.
- Dhananjay, B., and Chantal, K. (2006) Formation of more stable hydrophilic surfaces of PDMS by plasma and chemical treatments. *Microelectron Eng* **83**: 1277–1279.
- Duffy, D., McDonald, J., Schueller, O., and Whitesides, G. (1998) Rapid prototyping of microfluidic systems in poly(dimethylsiloxane). *Anal Chem* **70**: 4974–4984.
- Efimenko, K., Wallace, W., and Genzer, J. (2002) Surface modification of Sylgard-184 poly(dimethyl siloxane) networks by ultraviolet and ultraviolet/ozone treatment. *J Colloid Interface Sci* **254**: 306–315.
- Gabor, E.M., Vries, E.J., and Janssen, D.B. (2003) Efficient recovery of environmental DNA for expression cloning by indirect extraction methods. *FEMS Microbiol Ecol* **44**: 153–163.
- Handelsman, J. (2004) Metagenomics: application of genomics to uncultured microorganisms. *Microbiol Mol Biol Rev* **68**: 669–685.
- Ishmukhametov, R., Galkin, M., and Vik, S. (2005) Ultrafast purification and reconstitution of His-tagged cysteine-less *Escherichia coli* F1Fo ATP synthase. *Biochim Biophys Acta* **1706**: 110–116.
- Jing, Y., Wolfgang, A., Martin, F., Florian, H., Clemens, F., and Wilhelm, T. (2013) Monodisperse water-in-oil-in-water (W/O/W) double emulsion droplets as uniform compartments for high-throughput analysis via flow cytometry. *Micromachines* **4**: 402–413.
- Köster, S., Angilè, F., Duan, H., Agresti, J., Wintner, A., Schmitz, C., *et al.* (2008) Drop-based microfluidic devices for encapsulation of single cells. *Lab Chip* **8**: 1110–1115.
- Lahann, J., Balcells, M., Lu, H., Rodon, T., Jensen, K., and Langer, R. (2003) Reactive polymer coatings: a first step toward surface engineering of microfluidic devices. *Anal Chem* **75**: 2117–2122.
- Larsen, A., Dunn, M., Hatch, A., Sau, S., Youngbull, C., and Chaput, J. (2016) A general strategy for expanding polymerase function by droplet microfluidics. *Nat Commun* **7**: 11235.
- Lee, M., and Lee, S. (2013) Bioprospecting potential of the soil metagenome: novel enzymes and bioactivities. *Genomics Inform* **11**: 114–120.
- Li, S.B., Gong, X.Q., Nally, C.S., Zeng, M., Gaule, T., Anduix-Canto, C., *et al.* (2016) Rapid preparation of highly reliable PDMS double emulsion microfluidic devices. *RSC Adv* **6**: 25927–25933.
- Lim, S., and Abate, A. (2013) Ultrahigh-throughput sorting of microfluidic drops with flow cytometry. *Lab Chip* **13**: 4563–4572.
- Liu, N., Li, H., Chevrette, M., Zhang, L., Cao, L., Zhou, H., *et al.* (2018) Functional metagenomics reveals abundant polysaccharide-degrading gene clusters and cellobiose utilization pathways within gut microbiota of a wood-feeding higher termite. *ISME J* **13**: 104–117.
- Lorenz, P., and Eck, J. (2005) Metagenomics and industrial applications. *Nat Rev Microbiol* **3**: 510–516.
- Ma, F., Chung, M., Yao, Y., Nidetz, R., Lee, L., Liu, A., *et al.* (2018) Efficient molecular evolution to generate enantioselective enzymes using a dual-channel microfluidic droplet screening platform. *Nat Commun* **9**: 1030.
- Ma, F., Xie, Y., Huang, C., Feng, Y., and Yang, G. (2014) An improved single cell ultrahigh throughput screening method based on in vitro compartmentalization. *PLoS One* **9**: e89785.
- Manco, G., Giosuè, E., D'Auria, S., Herman, P., Carrea, G., and Rossi, M. (2000) Cloning, overexpression, and properties of a new thermophilic and thermostable esterase with sequence similarity to hormone-sensitive lipase subfamily from the Archaeon *Archaeoglobus fulgidus*. *Arch Biochem Biophys* **373**: 182–192.
- McDonald, J., and Whitesides, G. (2002) Poly(dimethylsiloxane) as a material for fabricating microfluidic devices. *Acc Chem Res* **35**: 491–499.
- Pierre, Y., Balint, K., Fabrice, G., Charlotte, M., Gerhard, F., Mark, F., *et al.* (2015) Ultrahigh-throughput discovery of promiscuous enzymes by picodroplet functional metagenomics. *Nat Commun* **6**: 10008.
- Renko, M., Taler-Vertič, A., Mihelič, M., Zerovnik, E., and Turk, D. (2014) Partial rotational lattice order–disorder in stefin B crystals. *Acta Crystallogr D Biol Crystallogr* **70**: 1015–1025.
- Simon, C., and Daniel, R. (2011) Metagenomic analyses: past and future trends. *Appl Environ Microbiol* **77**: 1153–1161.
- Trantidou, T., Elani, Y., Parsons, E., and Ces, O. (2017) Hydrophilic surface modification of PDMS for droplet microfluidics using a simple, quick, and robust method via PVA deposition. *Microsyst Nanoeng* **3**: 16091.
- Uchiyama, T., and Miyazaki, K. (2009) Functional metagenomics for enzyme discovery: challenges to efficient screening. *Curr Opin Biotechnol* **20**: 616–622.
- Wang, A., Xu, J., Zhang, Q., and Chen, H. (2006) The use of poly(dimethylsiloxane) surface modification with gold nanoparticles for the microchip electrophoresis. *Talanta* **69**: 210–215.
- Waterhouse, A., Bertoni, M., Bienert, S., Studer, G., Tauriello, G., Gumienny, R., *et al.* (2018) SWISS-MODEL: homology modelling of protein structures and complexes. *Nucleic Acids Res* **46**: W296–W303.
- Xia, Y., and Whitesides, G. (1998) Soft lithography. *Annu Rev Mater Sci* **28**: 153–184.
- Xu, Z., Xiang, S., Shu, W., Ju, C., Wei, H., Bang, C., *et al.* (2019) High-throughput screening of high lactic acid-

producing *Bacillus coagulans* by droplet microfluidic based flow cytometry with fluorescence activated cell sorting. *RSC Adv* **9**: 4507–4513.

Zinchenko, A., Devenish, S., Kintsjes, B., Colin, P., Fischlechner, M., and Hollfelder, F. (2014) One in a million: flow cytometric sorting of single cell-lysate assays in monodisperse picolitre double emulsion droplets for directed evolution. *Anal Chem* **86**: 2526–2533.

## Supporting Information

Additional Supporting Information may be found in the online version of this article at the publisher's web-site:

**Fig. S1.** The wettability of different materials. (A) Native PDMS, contact angle 105°. (B) Native glass, contact angle 57°. (C) PDMS modified by sequential layer-by-layer deposition of polyelectrolytes [Lab Chip, 2010, 10, 1814–1819; Anal. Chem. 2014, 86, 2526–2533], contact angle 63°. (D) PDMS treated with oxygen plasma contact angle 19°. (E) Plasma-treated PDMS exposed to air at room temperature for 2 h, contact angle 46°. (F) Plasma-treated PDMS exposed to air at room temperature for 4 h, contact angle 60°.

**Fig. S2.** The design of the secondary water-in-oil-in-water double emulsion droplet generation device. (A) 84 droplet generation units with flow-focusing junction could be contained in the same silicon wafer. (B) The fluidic channel of a single droplet generation unit, the red square referred to the flow-focusing junction. (C) The detailed structure of the flow-focusing junction.

**Fig. S3.** When using double-aqueous phase flow-focusing microfluidic device with the flow-focusing size of 15 μm and channel depth of 20 μm, (A) the performance of w/o single emulsion droplet generation, (B) the diameter of droplet (μm), and (C) droplet generation speed, under different flow rates of aqueous phase and oil phase. Scale bars: 100 μm, \*: unstable droplet generation.

**Fig. S4.** Model screening of active wild-type AFEST against inactive mutant M4. (A) Wild-type AFEST and inactive mutant M4 can be distinguished by growing on glycerol

tributyrate agar plates. (B) Fluorescent intensity distribution of micro-reactors encapsulating wild-type AFEST-expressing cells. (C) Fluorescent intensity distribution of micro-reactors encapsulating M4-expressing cells. (D-F) Fluorescent intensity distribution of micro-reactors encapsulating mixtures of wild-type AFEST-expressing cells and M4-expressing cells with ratios of 1:10, 1:100, and 1:1000 respectively. The sorting gate was illustrated in each mixture.

**Fig. S5.** Water-in-oil single emulsion droplets encapsulating *E. coli* cells. Arrows indicate cell-occupying droplets.

**Fig. S6.** Over-expression and purification of EstWY.

**Fig. S7.** The superposition of two models of EstWY constructed with their templates (Est U1 and Est-Y29) respectively. Residues in the black square showed the Ser-Lys-Tyr catalytic triads of models and of their relative templates. (A) Cyan, EstWY model constructed from Est U1; yellow, Est U1. (B) Light orange, EstWY model constructed from Est-Y29; light blue, Est-Y29.

**Fig. S8.** Sequence alignment of Est WY with its homologues (WP\_135283256.1 and WP\_148661411.1). The Ser-Lys-Tyr catalytic triad is only conserved in Est WY and its homologues, but not in other lipolytic families except Family VIII (only WP\_018062361.1 and YP\_001685768.1 in EstD2 Family are shown in this sequence alignment.). The conserved active site (Ser-Lys-Tyr) of Est WY and its homologues are indicated in red boxes with inverted red triangles.

**Table S1.** The thickness of the middle oil phase of w/o/w double emulsion droplets that were generated at different flow rates of the aqueous phase and the water-in-oil single emulsion phase.

**Table S2.** Enrichment of active wild-type AFEST against inactive mutant M4.

**Table S3.** The percentages of droplets encapsulating different amounts of cells at different cell/droplet ratios (calculated according to Poisson distribution).

**Table S4.** Esterases identified from metagenomic library using the flow cytometric droplet screening platform.

**Table S5.** Protein sequences of esterases identified in this work.